Title

Neuropathological correlates of structural and functional imaging biomarkers in 4-repeat tauopathies

Journal

Brain, 142(7)

ISSN

0006-8950

Authors

Spina, Salvatore
Brown, Jesse A
Deng, Jersey
et al.

Publication Date

2019-07-01

DOI

10.1093/brain/awz122

Peer reviewed

doi:10.1093/brain/awz122 BRAIN 2019: 142; 2068–2081 | 2068

BRAIN
A JOURNAL OF NEUROLOGY

Neuropathological correlates of structural and functional imaging biomarkers in 4-repeat tauopathies

Salvatore Spina,[1] Jesse A. Brown,[1] Jersey Deng,[1] Raquel C. Gardner,[1] Alissa L. Nana,[1] Ji-Hye L. Hwang,[1] Stephanie E. Gaus,[1] Eric J. Huang,[2] Joel H. Kramer,[1] Howie J. Rosen,[1] John Kornak,[3] John Neuhaus,[3] Bruce L. Miller,[1] Lea T. Grinberg,[1,2] Adam L. Boxer[1] and William W. Seeley[1,2]

Neurodegenerative dementia syndromes are characterized by spreading of pathological protein deposition along syndrome-specific neural networks. Structural and functional MRI measures can assess the integrity of these networks and have been proposed as biomarkers of disease progression for clinical trials. The relationship between *in vivo* imaging measures and pathological features, at the single subject level, remains largely unknown. Patient-specific maps of atrophy and seed-based intrinsic connectivity disruption, as compared to normal controls, were obtained for 27 patients subsequently diagnosed with progressive supranuclear palsy ($n = 16$, seven males, age at death 68.9 ± 6.0 years, imaging-to-pathology interval = 670.2 ± 425.1 days) or corticobasal degeneration ($n = 11$, two males, age at death 66.7 ± 5.4 years, imaging-to-pathology interval = 696.2 ± 482.2 days). A linear mixed effect model with crossed random effects was used to test regional and single-subject level associations between post-mortem regional measures of neurodegeneration and tau inclusion burden, on the one hand, and regional volume loss and seed-based intrinsic connectivity reduction, on the other. A significant association was found between tau inclusion burden and *in vivo* volume loss, at the regional level and independent of neurodegeneration severity, in both progressive supranuclear palsy [$n = 340$ regions; beta 0.036; 95% confidence interval (CI): 0.001, 0.072; $P = 0.046$] and corticobasal degeneration ($n = 215$ regions; beta 0.044; 95% CI: 0.009, 0.079; $P = 0.013$). We also found a significant association between post-mortem neurodegeneration and *in vivo* volume loss in both progressive supranuclear palsy ($n = 340$ regions; beta 0.155; 95% CI: 0.061, 0.248; $P = 0.001$) and corticobasal degeneration ($n = 215$ regions; beta 0.277; 95% CI: 0.104, 0.450; $P = 0.002$). We found a significant association between regional neurodegeneration and intrinsic connectivity dysfunction in corticobasal degeneration ($n = 215$ regions; beta 0.074; 95% CI: 0.005, 0.143; $P = 0.035$), but no other associations between post-mortem measures of tauopathy and intrinsic connectivity dysfunction reached statistical significance. Our data suggest that *in vivo* structural imaging measures reflect independent contributions from neurodegeneration and tau burden in progressive supranuclear palsy and corticobasal degeneration. Seed-based measures of intrinsic connectivity dysfunction showed less reliable predictive value when used as *in vivo* biomarkers of tauopathy. The findings provide important guidance for the use of imaging biomarkers as indirect *in vivo* assays of microscopic pathology.

1 Memory and Aging Center, Department of Neurology, University of California San Francisco, USA
2 Department of Pathology, University of California San Francisco, USA
3 Department of Epidemiology and Biostatistics, University of California San Francisco, USA

Correspondence to: William W. Seeley, MD
Memory and Aging Center
Department of Neurology
University of California, San Francisco
675 Nelson Rising Lane, Suite 190

Received August 8, 2018. Revised February 23, 2019. Accepted March 7, 2019. Advance Access publication May 12, 2019

San Francisco, CA 94158, USA
E-mail: Bill.Seeley@ucsf.edu

Keywords: tau; neuropathology; biomarkers of neurodegeneration; progressive supranuclear palsy; corticobasal degeneration

Abbreviations: CBD = corticobasal degeneration; PSP = progressive supranuclear palsy; PSP-RS = progressive supranuclear palsy-Richardson's syndrome

Introduction

Neurodegenerative dementia syndromes reflect the selective targeting of distinct large-scale neuronal networks, and progression is hypothesized to reflect disease propagation along anatomical and functional pathways of brain connectivity (Seeley *et al.*, 2009; Raj *et al.*, 2012; Zhou *et al.*, 2012; Gardner *et al.*, 2013; Guo *et al.*, 2013; Mandelli *et al.*, 2016; Collins *et al.*, 2017; Hoenig *et al.*, 2018). A sequence of molecular events including pathological protein folding, corruptive templating, and transsynaptic spreading has been proposed as a fundamental mechanism of disease spread within selectively vulnerable neuronal networks (Hyman *et al.*, 1984; Clavaguera *et al.*, 2009; de Calignon *et al.*, 2012; Liu *et al.*, 2012). In the tauopathies, specific morphological and cell type-specific patterns of pathological tau deposition define the diseases.

Structural MRI and task-free functional MRI are appealing methodologies for disease progression monitoring in neurodegenerative dementia syndromes because they are non-invasive, low cost, and can be obtained longitudinally without significant safety concerns. Structural MRI has been proposed as a surrogate biomarker for monitoring of disease progression in Alzheimer's disease clinical trials (Jack *et al.*, 2013), as well as in longitudinal studies of subjects at risk for frontotemporal dementia (FTD) (Rohrer *et al.*, 2015; Cash *et al.*, 2018). Both increased and decreased task-free functional MRI connectivity have been described within the default mode network of subjects across the continuum spanning from normal ageing to Alzheimer's disease (Greicius *et al.*, 2004; Buckner *et al.*, 2005; Zhou *et al.*, 2008; Zhang *et al.*, 2010; Wang *et al.*, 2013). Extensive literature has described functional intrinsic connectivity patterns in patients with FTD syndromes (Seeley *et al.*, 2007; Zhou *et al.*, 2010, 2017; Whitwell *et al.*, 2011*b*; Borroni *et al.*, 2012; Farb *et al.*, 2013; Filippi *et al.*, 2013; Guo *et al.*, 2013; Pievani *et al.*, 2014), and longitudinal changes have been investigated as potential biomarkers of disease progression for clinical trials for Alzheimer's disease and FTD (Zhang *et al.*, 2010; Goveas *et al.*, 2011; Sperling *et al.*, 2014; Serra *et al.*, 2016; Brown *et al.*, 2017).

Despite widespread interest in these biomarkers for clinical trial planning and dementia research (Boxer *et al.*, 2017; Whitwell *et al.*, 2017), little is known about the relationship between imaging measures of brain atrophy or intrinsic connectivity dysfunction and corresponding neuropathological changes, with most studies focusing on Alzheimer's disease, primary age-related tauopathy and Lewy body disease (Jack *et al.*, 2002; Whitwell *et al.*, 2008; Burton *et al.*, 2009; Josephs *et al.*, 2017). No such studies have been carried out in FTD or for any disease using functional MRI.

In this study, we assessed the relationships between *in vivo* volumetric and intrinsic connectivity imaging measures and post-mortem measures of neurodegeneration and tau inclusion burden. We assessed these relationships across brain regions and within individuals in patients with pathological diagnoses of progressive supranuclear palsy (PSP) or corticobasal degeneration (CBD), the two most common sporadic 4-repeat tauopathies.

Materials and methods

Subjects

Patients

We searched the University of California at San Francisco (UCSF) Neurodegenerative Disease Brain Bank database for patients with a primary pathological diagnosis of PSP or CBD, regardless of clinical syndrome (Litvan *et al.*, 1996*b*; Dickson *et al.*, 2002). Patients were included if they had been enrolled in UCSF Memory and Aging Center (MAC) longitudinal research projects during life, underwent standardized clinical, behavioural, and neuroimaging data collection, and had research quality structural T_1 MRI and task-free functional MRI available. This search led to the identification of 26 patients with PSP and 20 patients with CBD cases. To study the association between the primary proteinopathy (4-repeat tau) inclusion burden with ante-mortem imaging measures, we excluded patients with coexisting Alzheimer's disease neuropathological change intermediate or higher, Braak neurofibrillary tangle stage >3, any extent of Lewy body disease or TDP-43 proteinopathy, or evidence of vascular brain injuries within regions of interest (Braak and Braak, 1991; McKeith *et al.*, 1996; Mackenzie *et al.*, 2010*b*; Montine *et al.*, 2012). Patients with coexisting argyrophilic grain disease (Ferrer *et al.*, 2008) were included because of the high prevalence of this diagnosis in ageing, PSP, and CBD (Rodriguez *et al.*, 2016; Gil *et al.*, 2018). When more than one neuroimaging assessment was available, we used the one closest to death. When this imaging study did not pass quality control, the passing MRI scan next nearest to death was used. This method led to the identification of 16 patients with pathologically diagnosed PSP and 11 with CBD. The imaging-to-pathology interval was 670.2 ± 425.1 days in PSP and 696.2 ± 482.2 days in CBD. Demographics, clinical,

functional and pathological data are described in Table 1 (Pfeffer *et al.*, 1982; Fahn *et al.*, 1987).

Control groups

A group of 288 healthy control subjects (healthy control group 1: 250 right-handed, three ambidextrous; 116 male; age at imaging 65.8 ± 10.8 years) was identified for the structural neuroimaging analyses from a cohort of MAC research participants. A subgroup of healthy control group 1, comprising 165 subjects (healthy control group 2: 140 right-handed, two ambidextrous; 64 male; age at imaging 66.2 ± 11.4 years) with available task-free functional MRI studies was used as controls for the functional neuroimaging analyses.

Consent

All participants or their caregivers provided written informed consent for the study according to the Declaration of Helsinki, which was approved by the UCSF Committee on Human Research.

Neuropsychological assessment

Patients and controls underwent a standard battery of neuropsychological tests as described previously (Perry *et al.*, 2017). Interval time between imaging and neuropsychological testing was 2 ± 109 days in the PSP cohort and 96 ± 142 days in the CBD cohort. Group-level cognitive performances for PSP, CBD, and controls are summarized in Supplementary Table 1.

Neuropathology

Post-mortem brains were freshly cut according to an interleaved bi-hemispheric coronal slabbing protocol that captures 13 (±1) fixed coronal slabs for histological processing and 12 (±1) frozen slabs for biochemical/molecular biological analysis. Cerebella were cut into sagittal sections and brainstems into axial sections. Following 72-h formalin fixation, cerebral and cerebellar slabs were dissected to generate 20 standard regional tissue blocks (encompassing 27 regions of interest) used for all histopathological studies (Supplementary Fig. 1). Eight-micrometre thick formalin-fixed paraffin-embedded sections were cut from each block and stained with haematoxylin and eosin and with immunohistochemistry for hyperphosphorylated tau, amyloid-β, TDP-43, alpha-synuclein, and 3R-tau antibodies (to identify Alzheimer's disease-related tau deposition in the context of a primary 4-repeat tauopathy) (de Silva *et al.*, 2003; Tartaglia *et al.*, 2010). Neuropathological diagnoses were rendered according to published criteria (Litvan *et al.*, 1996*b*; McKeith *et al.*, 1996; Dickson *et al.*, 2002; Mackenzie *et al.*, 2010*a*; Montine *et al.*, 2012). For

Table 1 Demographic, clinical and pathological characteristics of the patients in the study

Subject	Pathological diagnosis	Clinical diagnosis	Sex	Age at death, years	Education, years	Handedness	Disease duration, years	UPDRS motor score	FAQ Score	Imaging to pathology, days	Thal Phase	AD Braak	LBD Braak	Other pathologies
1	PSP	PSP-RS	M	69.4	20	Right	6	53	n.a.	104	0	0	0	AGD
2	PSP	PSP-RS	M	76.8	20	Right	10	61[b]	n.a.	844	0	2	0	AGD, VBI
3	PSP	PSP-RS	F	72.8	13	Right	6	46	n.a.	574	0	1	0	VBI
4	PSP	PSP-RS	F	66.5	18	Left	8	58[b]	15	895	0	1	0	–
5	PSP	PSP-RS[a]	F	66.7	16	Right	7	34	14	1336	2	1	0	CAA
6	PSP	PSP-RS[a]	M	70.0	16	Right	9	36	9	1401	0	2	0	VBI
7	PSP	PSP-RS	F	56.4	14	Right	6	n.a.	n.a	639	2	2	0	–
8	PSP	PSP-RS	M	74.7	20	Right	10	15	5	1365	0	3	0	AGD
9	PSP	PSP-RS	F	69.2	21	Left	7	26	14	246	1	2	0	AGD
10	PSP	PSP-RS[a]	F	70.3	12	Right	10	64	28	334	3	2	0	VBI
11	PSP	PSP-RS[a]	F	68.7	18	Right	18	24	20	276	2	3	0	CAA
12	PSP	PSP-RS	M	59.0	14	Right	7	16	21	710	2	1	0	–
13	PSP	PSP-RS	M	63.0	18	Right	9	41	17	820	2	1	0	AGD
14	PSP	PSP-RS	F	66.2	14	Right	9	42[b]	13	254	0	2	0	–
15	PSP	PSP-RS	M	77.6	16	Right	5	17	16	231	2	2	0	VBI
16	PSP	PSP-RS	F	75.0	16	Right	6	62[b]	23	695	1	2	0	AGD
17	CBD	bvFTD	M	63.8	15	Right	6	16	28	629	2	2	0	CAA
18	CBD	CBS	F	64.5	16	Right	7	48	8	972	0	1	0	VBI
19	CBD	bvFTD	F	73.3	17	Right	6	14	17	1344	1	1	0	–
20	CBD	PSP-RS	F	67.6	16	Right	4	43[b]	30	220	1	2	0	VBI
21	CBD	PSP-RS	M	60.6	14	Right	6	n.a.	n.a.	428	2	1	0	–
22	CBD	CBS	F	62.0	16	Right	7	45	12	435	1	0	0	VBI
23	CBD	CBS	F	63.4	18	Right	8	30	8	723	1	1	0	
24	CBD	CBS	F	64.1	18	Right	5	42[b]	6	326	1	2	0	AGD, CAA
25	CBD	CBS	F	77.6	16	Right	8	31	15	432	2	2	0	AGD, VBI
26	CBD	PSP-RS	F	64.4	16	Right	4	15	24	380	0	1	0	–
27	CBD	bvFTD	F	72.4	18	Right	8	4	5	1769	5	2	0	VBI

AGD = argyrophilic grain disease; CAA = cerebral amyloid angiopathy; CBD = corticobasal degeneration; bvFTD = behavioural variant frontotemporal dementia; F = female; FAQ = Functional Activities Questionnaire; M = male; n.a. = not available; PSP-RS = probable PSP-RS with clinical diagnosis of PSP using the movement disorder society criteria (Höglinger *et al.*, 2017); UPDRS = Unified Parkinson's disease rating scale; VBI = vascular brain injury.

[a]Possible PSP-RS with clinical diagnosis of PSP using the movement disorder society criteria (Höglinger *et al.*, 2017).

[b]Does not include untestable items.

every region of interest, neuronal loss was graded as: 0 (⩽50%), 1 (50–70%), 2 (71–90%) and 3 (⩾90%) estimated loss. Astrogliosis was graded as 0 (absent), 1 (mild), 2 (moderate), and 3 (severe). Microvacuolation was graded on the same scale but only for cerebral cortical regions. A neurodegeneration score (ND) was calculated for every cortical region of interest as follows: ND = [(gliosis + microvacuolation) / 2] + neuronal loss. For subcortical and brainstem regions of interest, astrogliosis and neuronal loss scores were added. Regional tau inclusion burden scores were calculated by summing semi-quantitative scores on the same 4-point scale for each pathological hallmark (i.e. neurofibrillary tangles, neuronal cytoplasmic inclusions, tufted astrocytes, astrocytic plaques, thorny astrocytes, oligodendroglial coiled bodies, cortical neuropil threads and white matter threads).

Imaging acquisition

MRI scans from patients and healthy controls were obtained at the UCSF Neuroscience Imaging Center on a Siemens Trio 3.0 T scanner. T_1-weighted magnetization-prepared rapid gradient-echo (MP-RAGE) structural scans were acquired with an acquisition time = 533 s, sagittal orientation, a field of view of 160 × 240 × 256 mm with an isotropic voxel resolution of 1 mm^3, repetition time = 2300 ms, echo time = 2.98 ms, inversion time = 900 ms, flip angle = 9°. Task-free T_2*-weighted echo planar functional MRI scans were acquired with an acquisition time = 486 s, axial orientation with interleaved ordering, field of view = 230 × 230 × 129 mm, matrix size = 92 × 92, effective voxel resolution = 2.5 × 2.5 × 3.0 mm, repetition time = 2000 ms, echo time = 27 ms, for a total of 240 volumes.

MRI processing

T_1-weighted scans were visually inspected to exclude scans with poor quality and obvious artefact. Images were then processed using the SPM12 default estimation settings for segmentation into grey and white matter and spatial normalization to the standard SPM tissue probability maps. Images were modulated, corrected for non-linear warping only, and smoothed with a 8 mm full-width at half-maximum isotropic Gaussian kernel. Functional MRI scans were preprocessed using a protocol described previously (Brown *et al.*, 2017). Scans were excluded if head motion was >3 mm of maximum relative translation, >3° of maximum relative rotation, and higher than 10% of frames with motion 'spikes' >1 mm.

Imaging region of interest selection

To assess imaging-to-pathology correlations at the single subject level in each of the 27 histological regions of interest, we used a standardized algorithm for identifying the imaging region of interest that best matched our standard neuropathological dissections, similar to previous approaches (Raman *et al.*, 2016). To create a standard set of regions of interest for this and future studies, we elected to use the Human Brainnetome Atlas, a validated connectivity-based parcellation atlas composed of 210 cortical and 36 subcortical brain regions, classified by means of non-invasive multimodal structural, task-free functional, and diffusion MRI methods (Fan *et al.*, 2016). This atlas does not contain parcels for the cerebellum and the brainstem, therefore dentate nucleus, substantia nigra and tectum regions of interest were manually drawn on the MNI T_1 template using MRIcron mirroring our standard blocking protocol (Rorden and Brett, 2000).

To select Brainnetome parcels that best matched our remaining standard histological dissections, we first used MRIcron to manually draw MNI T_1 template regions of interest mirroring our standard dissections. We then assigned each drawn region of interest to the Brainnetome parcel with the highest voxel overlap in MNI space. Fifteen drawn regions of interest were uniquely assigned to a single Brainnetome parcel. Drawn regions of interest covering amygdala, superior/middle temporal gyrus, thalamus, calcarine cortex, and entorhinal cortex were better represented by combining two to three Brainnetome parcels each in order to cover the entire volume of the region assessed neuropathologically (Table 2). Suitable Brainnetome parcels matching the standard dissections of the frontal pole, globus pallidus, and subthalamic nucleus were not available; therefore, for these regions we used the drawn region of interest parcels. Drawn region of interest parcels were also used for the dentate nucleus, substantia nigra, tectum and periaqueductal grey, which are not represented in the Brainnetome atlas. The substantia nigra region of interest included the entire extent of the nuclei bilaterally. The final list of Brainnetome parcels corresponding to brain regions of interest is provided in Table 2. Once all regions were chosen, we calculated the mean grey matter and white matter tissue probability map value for each region of interest to assign each region to either the grey or white matter segment, according to whichever segment returned a higher value, for the purposes of volume assessment. For functional connectivity maps, we extracted the region of interest mean connectivity values (parameter estimates). Globus pallidus, thalamus, subthalamic nucleus, dentate nucleus, substantia nigra, and midbrain tectum were assigned to the white matter segment. All remaining regions were assigned to the grey matter segment.

Imaging analyses

Structural MRI data were analysed using voxel-based morphometry. Intrinsic connectivity dysfunction was assessed using seed-based intrinsic connectivity methods, centred on anatomical areas targeted in each disease, following previously described approaches (Seeley *et al.*, 2009; Gardner *et al.*, 2013). For the PSP group, we chose a 4-mm radius sphere centred on the midline in the rostral midbrain tegmentum, since the network anchored by this region has been described previously and mirrors the anatomical vulnerability pattern in PSP (Boxer *et al.*, 2006; Gardner *et al.*, 2013). For the CBD group, the superior frontal sulcus parcel from the Brainnetome atlas was selected since it corresponded to the peak of atrophy, within cortical regions sampled pathologically, in both the subgroup of seven CBD patients with left-predominant atrophy and in the subgroup of four CBD patients with right-predominant atrophy (Supplementary Fig. 2). For each subject, grey matter volumes and connectivity parameters were measured within the regions of interest in the cerebral hemisphere with the higher extent of atrophy and in the contralateral dentate nucleus, corresponding to the sides prospectively chosen for pathological assessment and scoring. For superior frontal sulcus-seeded intrinsic connectivity measures in CBD, the seed was ipsilateral to the cerebral regions of interest and contralateral to the dentate nucleus. We calculated the average

Table 2 List of Brainnetome parcels and hand-drawn regions of interest

Region of interest	Brainnetome parcels and hand-drawn regions of interest	
	Left hemisphere	Right hemisphere
Frontal pole	Hand-drawn	Hand-drawn
Anterior orbital gyrus	45	46
Anterior mid-cingulate gyrus	179	180
Subgenual cingulate gyrus	187	188
Posterior cingulate gyrus	175	176
Middle frontal gyrus	15	16
Inferior frontal gyrus	39	40
Superior frontal sulcus	25	26
Superior and middle temporal gyrus	75 + 87	76 + 88
Inferior temporal gyrus	93	94
Insula	171	172
Precentral gyrus	57	58
Postcentral gyrus	159	160
Angular gyrus	141	142
Calcarine cortex	191 + 193	192 + 194
Cornus ammonis	217	218
Entorhinal cortex	109 + 111	110 + 112
Ventral striatum	219	220
Putamen	229	230
Globus pallidus	Hand-drawn	Hand-drawn
Amygdala	211 + 213	212 + 214
Thalamus	235 + 239 + 241	236 + 240 + 242
Subthalamic nucleus	Hand-drawn	Hand-drawn
Substantia nigra	Hand-drawn	Hand-drawn
Midbrain tectum	Hand-drawn	Hand-drawn
Periaqueductal gray	Hand-drawn	Hand-drawn
Dentate nucleus	Hand-drawn	Hand-drawn

blood oxygen level-dependent signal intensity of all voxels within these regions of interest at each repetition time over each subject's 8-min scan. The resulting time series were used as covariates of interest in a whole-brain statistical parametric regression analysis using SPM12 to derive images corresponding to the region of interest's intrinsic functional correlation map for each subject. Voxelwise regression was used to estimate mean W-score maps of grey matter loss and intrinsic connectivity dysfunction within patient regions of interest, taking into consideration age, sex, handedness, total intracranial volume and years of education, for both modalities, as well as education for functional W-maps. Structural W-maps were calculated using the healthy control group 1 and functional W-maps using the healthy control group 2. W-scores are analogous of Z-scores accounting for multiple covariates at the same time. This method provides a voxelwise metric of a patient's deviation from an expected imaging value based on the relevant factors in the control group (La Joie *et al.*, 2012).

Statistical analyses

To test the independent association of pathological measures and *in vivo* MRI biomarkers, we used linear mixed effect models in order to account for repeated measures from the same patient. Outcomes were *in vivo* measures of grey or white matter volume and seed-based intrinsic connectivity dysfunction at the single patient level. Fixed effects predictors were regional neurodegeneration and tau inclusion burden, age, sex, disease duration, and elapsed time between MRI and death. Random effects predictors were patient identity and region of interest, both of which have their own specific variance. We elected to cross the random effects in order to simultaneously incorporate the following two assumptions: (i) different regions within a subject behave more similarly than different regions in different subjects; and (ii) the same regions in different subjects behave more similarly than different regions in different subjects. Importantly, the crossed model allows for different levels of correlation within subject across regions versus within region across subjects. Because region of interest and patient identity effects are unlikely to be completely independent, we acknowledge that this assumption must be regarded as an approximation. We would argue, however, that the crossed random effect structure is a better assumption than a region-within-subject nested configuration, which would not acknowledge the correlation that exists within a region across subjects (Baayen *et al.*, 2008). The default option in STATA was used, which fits the model with maximum likelihood. Fixed effects were included in additive fashion. To determine whether elapsed time between MRI and death interacted with neuropathological predictors, we assessed these interactions statistically within each model and

added interaction terms when they showed a statistically significant effect on the neuroimaging outcomes. A statistically significant interaction between neurodegeneration score and elapsed time between MRI and death was found in the model predicting regional volume loss in CBD, and therefore the interaction term was added to this model. Since no other statistically significant interactions were found between pathological measures and elapsed time between MRI and death, in the interest of parsimoniously representing models, no interaction terms were added to the remaining models. The same models were re-run to assess the independent associations between tau subscores (i.e. total neuronal tau, and total glial tau), instead of the total tau score, and MRI findings.

To assess the relationship between pathological measures and elapsed time from imaging to death, in both cohorts, we used linear mixed-effect models with crossed random effects. Outcomes were either neurodegeneration score or tau score. Fixed effects predictors were neurodegeneration score or tau score (if not used as a primary outcome), age, sex, disease duration in years and imaging-to-death elapsed time in years. An interaction factor between the neuropathological outcome of interest and elapsed time from imaging to death in years was also added to the model. Crossed random effects were patients identity and anatomical regions of interest.

A nominal significance level of $\alpha = 0.05$, $P < 0.05$ was used throughout. Although we examined multiple correlations, we report nominal P-values without adjustment for multiple testing since such adjustment would be focused on avoidance of one or more results with $P < 0.05$ in the case where all correlations are truly zero, which is an unlikely hypothesis. We therefore rely on scientific judgment to indicate where caution is warranted despite findings with $P < 0.05$ (Rothman, 1990; Savitz and Olshan, 1995; Perneger, 1998; Bacchetti, 2002). Diagnostic plot analyses were carried out to rule out any violation of linearity assumptions and to confirm the approximate normal distribution of residuals in all mixed effect models. All analyses were performed in STATA 14.

Data availability

All data used in this study are available for review upon request.

Results

Patient demographics

All 16 patients with PSP (seven males, nine females) had been clinically diagnosed with either probable ($n = 12$) or possible ($n = 4$) PSP-Richardson syndrome (PSP-RS), according to published criteria (Litvan *et al.*, 1996*a*). The 11 patients with CBD (two males, nine females) had received various clinical syndromic diagnosis antemortem: five had been diagnosed with corticobasal syndrome, three with behavioural variant frontotemporal dementia (bvFTD), and three with probable PSP-RS (Litvan *et al.*, 1996*a*; Rascovsky *et al.*, 2011; Armstrong *et al.*, 2013). Patient demographics and information regarding coexisting Alzheimer's disease and other comorbid pathological changes are summarized in Table 1. Coexisting argyrophilic grain disease was observed in 6/16 patients with PSP and 2/11 patients with CBD, consistent with the high prevalence of this co-pathology in non-demented older subjects (Rodriguez *et al.*, 2016) and in PSP and CBD (Gil *et al.*, 2018). Neurodegeneration scores were available for 423/432 patient-regions in the PSP cohort, and 293/297 patient-regions in the CBD cohort. Tau inclusion burden scores were available for 340/432 patient-regions in the PSP cohort and 215/297 patient-regions in the CBD cohort. Missing measures were randomly distributed across patients and regions, therefore unlikely to have unduly influenced the results.

The relationship between regional tissue dissection, Brainnetome parcels, and single-subject W-score maps of grey and white matter atrophy, as well as intrinsic connectivity dysfunction in a representative patient with PSP are illustrated in Fig. 1. Group-level W-score maps of grey and white matter atrophy, and intrinsic connectivity dysfunction in the PSP and CBD groups are described in Fig. 2. W-score variance within regions and among subjects is described in Supplementary Fig. 3. The associations between demographics covariates and regional grey matter volume loss or intrinsic connectivity dysfunction are described in the Supplementary material, Results section.

Neurodegeneration and tau inclusion burden independently predict *in vivo* brain atrophy

First, we assessed the relationships between structural MRI and neuropathological findings. In PSP, neurodegeneration scores predicted *in vivo* brain atrophy (grey matter W-score) at the regional level, after controlling for tau inclusion burden and other covariates [$n = 340$ regions; beta 0.155; 95% confidence interval (CI): 0.061, 0.248; $P = 0.001$] (Fig. 3A). In addition, we observed a statistically significant relationship between tau inclusion burden and *in vivo* brain atrophy, independent of neurodegeneration severity and other covariates ($n = 340$ regions; beta 0.036; 95% CI: 0.001, 0.072; $P = 0.046$) (Fig. 3C).

CBD patients showed similar results to those for PSP. We observed a statistically significant association between neurodegeneration and atrophy, after adjusting for tau inclusion burden and other covariates ($n = 215$; beta 0.277; 95% CI: 0.104, 0.450; $P = 0.002$) (Fig. 3B). In addition, tau inclusion burden predicted *in vivo* brain atrophy, independent of neurodegeneration severity and other covariates ($n = 215$; beta 0.044; 95% CI: 0.009, 0.079; $P = 0.013$) (Fig. 3D).

Pathological variables did not predict intrinsic connectivity dysfunction in PSP

PSP-RS is associated with a targeted intrinsic connectivity network, anchored by the rostral midbrain tegmentum, and

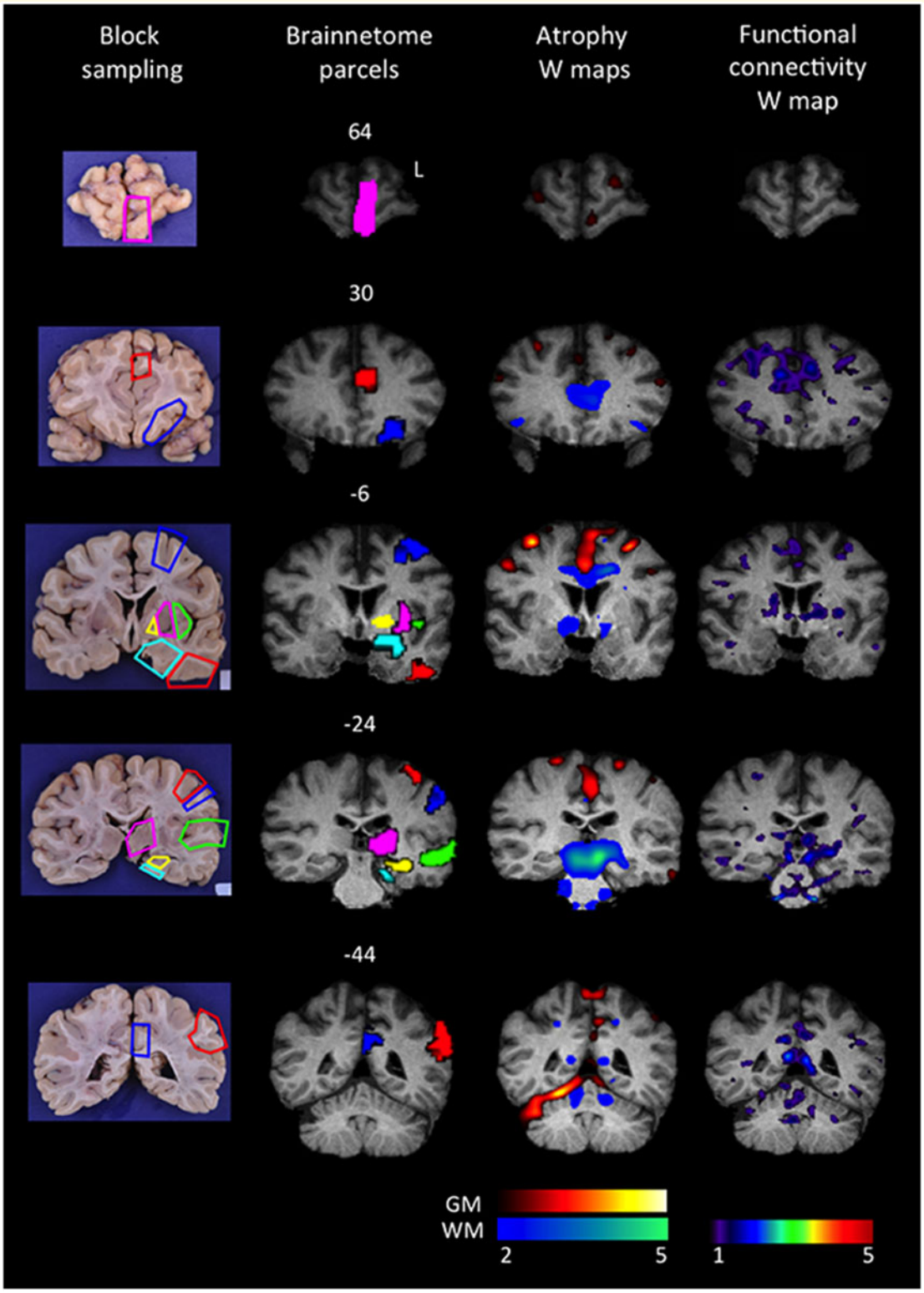

Figure 1 Regions of interest: anatomical tissue sampling, Brainnetome parcels, and single-subject W-score maps of atrophy and intrinsic connectivity dysfunction in a PSP patient. From *left* to *right*, depicted is the relationship between regional tissue dissection, corresponding Brainnetome Atlas parcels, W-maps of grey and white matter atrophy, and seed-based intrinsic connectivity dysfunction. In the *top row*, the frontal pole region of interest is indicated in purple. In the *second row*, the anterior mid-cingulate gyrus is in red, and the anterior orbital gyrus is in blue. In the *third row*, the superior frontal sulcus is in blue, the insular cortex is in green, the putamen is in purple, the globus pallidus is in yellow, the amygdala is in cyan and the inferior temporal gyrus is in red. In the *fourth row*, the precentral gyrus is in red, the postcentral gyrus is in blue, the thalamus is in purple, the superior and middle temporal gyrus are in green, the cornus ammonis is in yellow, and the entorhinal cortex is in cyan. In the *bottom row*, the posterior cingulate gyrus is in blue and the angular gyrus is in red. Corresponding colour bars for grey matter W-score (GM), white matter W-score (WM) and functional connectivity W-score maps are indicated. Higher W-scores correspond to higher extent of volume loss or connectivity reduction (Rorden and Brett, 2000).

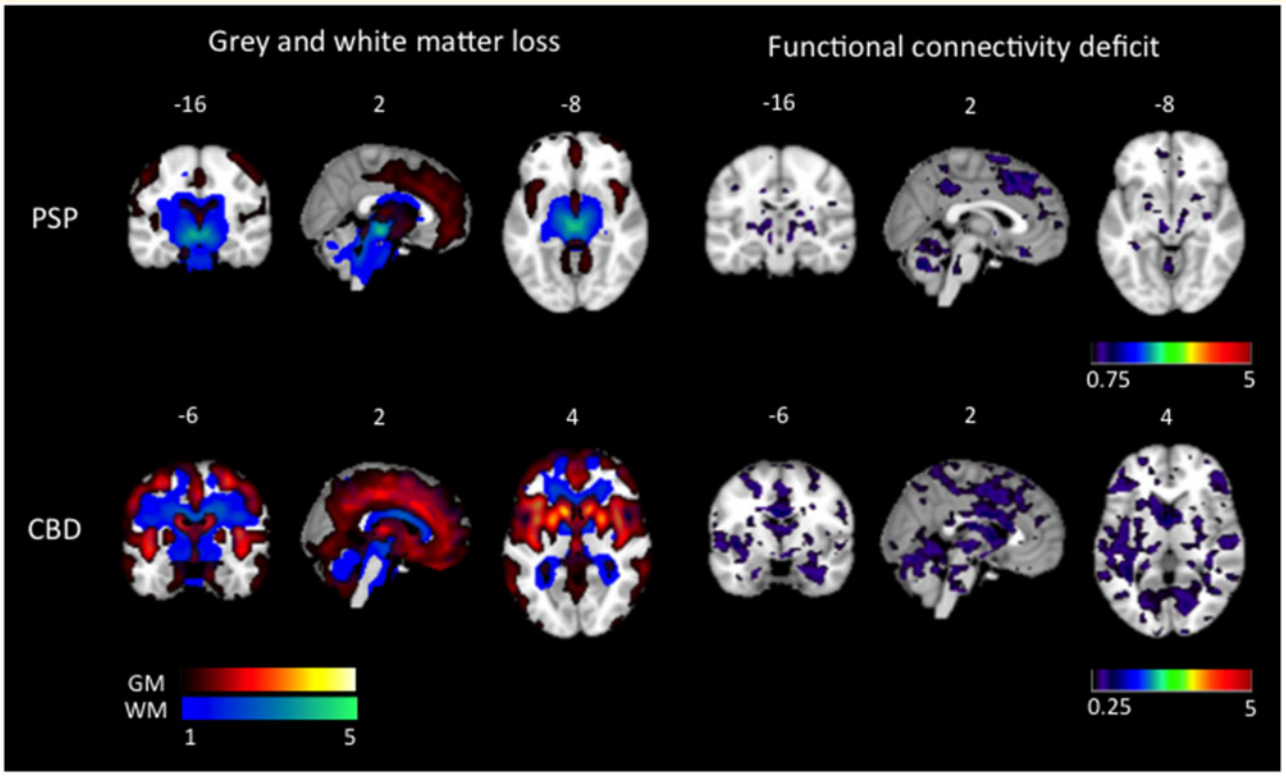

Figure 2 Group level W-score maps of atrophy and connectivity dysfunction in PSP and CBD. Heat bars for grey matter W-score (GM), white matter W-score (WM), and connectivity W-score. Higher W-scores correspond to higher extent of volume loss or connectivity reduction (Rorden and Brett, 2000).

a cross-sectional analysis linked reduced connectivity within this network to worsening clinical deficits (Gardner *et al.*, 2013). Nonetheless, in PSP the associations between regional rostral midbrain tegmentum-seeded intrinsic connectivity mean W-scores and neurodegeneration scores ($n = 340$; beta 0.041; 95% CI: −0.010, 0.093; $P = 0.118$) (Fig. 3E) or tau inclusion burden ($n = 340$; beta 0.010; 95% CI: −0.010, 0.029; $P = 0.321$) did not reach statistical significance (Fig. 3G), although the associations were in the expected direction.

Neurodegeneration scores, not tau inclusion burden, predicts intrinsic connectivity dysfunction in CBD

In CBD, no previous study has assessed intrinsic connectivity directly. Here, the intrinsic connectivity disruptions observed were mild, perhaps not surprisingly given the small, clinically heterogeneous CBD sample. Nonetheless, we observed a statistically significant positive association between regional superior frontal sulcus-seeded intrinsic connectivity mean W-scores and the neurodegeneration score ($n = 215$; beta 0.074; 95% CI: 0.005, 0.143; $P = 0.035$) (Fig. 3F) independent from other covariates. The association between regional superior frontal sulcus-seeded intrinsic connectivity mean W-scores and tau inclusion burden ($n = 215$; beta −0.011; 95% CI: −0.032, 0.009; $P = 0.288$) (Fig. 3H) was not in the expected direction and did not reach statistical significance.

Relationship between neuronal or glial subscores of tau pathological burden and imaging biomarkers

In the PSP cohort, neuronal tau burden was an independent predictor of ante-mortem structural atrophy ($n = 340$; beta 0.167; 95% CI: 0.079, 0.255; $P < 0.001$), while the association between glia tau burden and structural atrophy did not reach statistical significance ($n = 340$; beta −0.010; 95% CI: −0.072, 0.052; $P = 0.749$). In contrast, in the CBD cohort we observed a trend toward statistical significance between glial tau burden and structural atrophy ($n = 215$; beta 0.082; 95% CI: −0.001, 0.165; $P = 0.054$), while the association between neuronal tau burden and structural atrophy was not significant ($n = 215$; beta 0.013; 95% CI: −0.137, 0.162; $P = 0.870$).

The association between subscores of tau burden and connectivity dysfunction measures is of more complex interpretation. In the PSP cohort, both neuronal tau burden

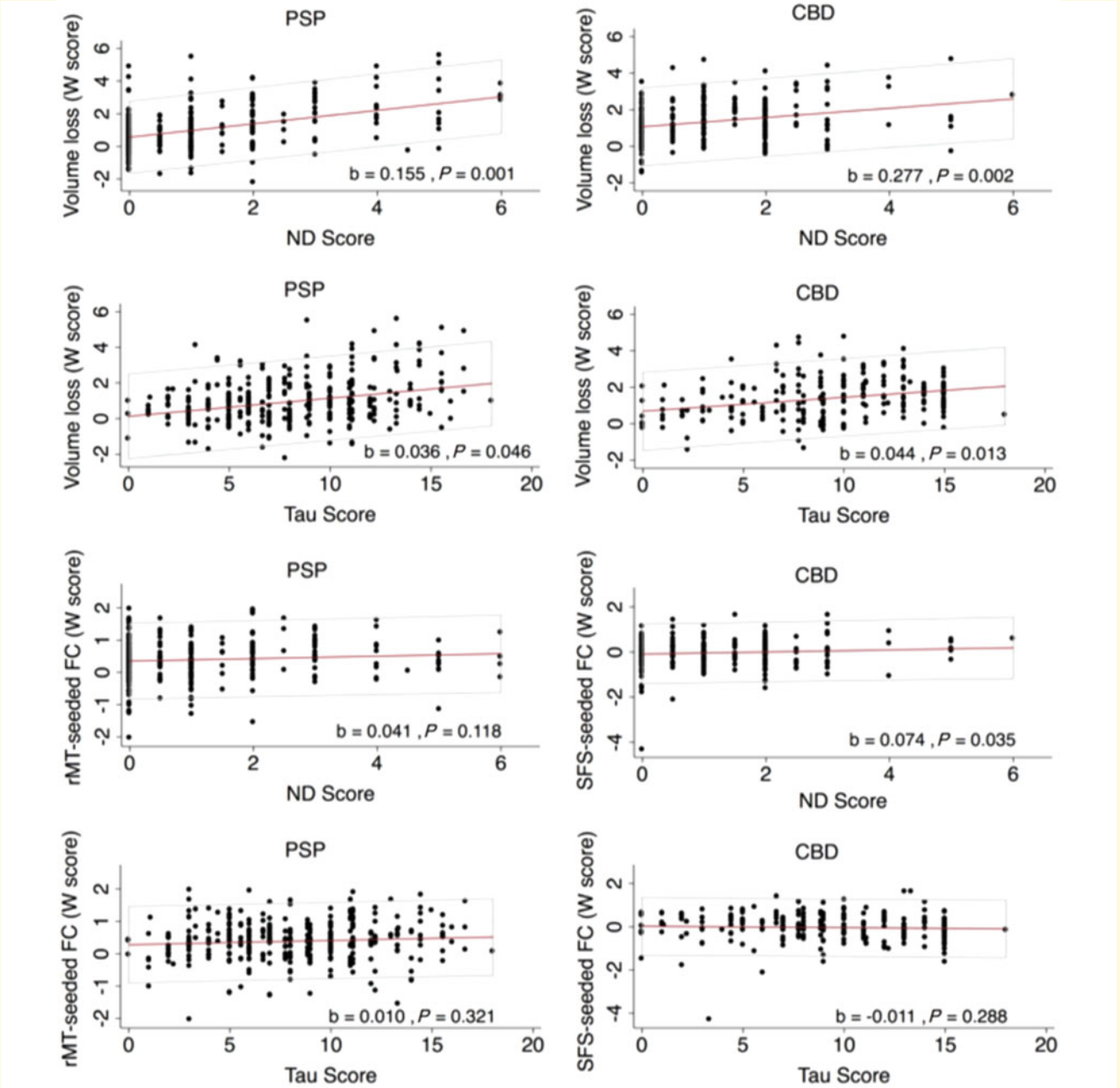

Figure 3 Scatter plots displaying the regional association between neurodegeneration and tau scores with W-scores of structural and intrinsic connectivity dysfunction. FC = functional connectivity. Dots represent linear prediction; boxed area represents 95% CI; red line indicates fitted values.

($n = 340$; beta −0.053; 95% CI: −0.099, −0.006; $P = 0.026$) and glial tau burden ($n = 340$; beta 0.055; 95% CI: 0.024, 0.086; $P < 0.001$) independently predicted connectivity dysfunction, but these effects, both relatively small, were in opposite directions. No significant association between neuronal tau burden ($n = 215$; beta 0.023; 95% CI: −0.064, 0.110; $P = 0.602$) or glial tau burden ($n = 215$; beta −0.036; 95% CI: −0.083, 0.011; $P = 0.133$) and connectivity dysfunction was observed in the CBD cohort.

Relationship between pathological measures and interval time between imaging and death

PSP patients who came to autopsy after a long interval since MRI showed greater regional neurodegeneration scores ($n = 340$; beta 0.291/year; 95% CI: 0.268, 0.314; $P < 0.001$) and tau burdens ($n = 340$; beta 0.030/year; 95% CI: 0.004, 0.056; $P = 0.025$), as expected. In the CBD cohort we also observed a significant association

between imaging-to-death interval and neurodegeneration score ($n = 215$; beta 0.352/year; 95% CI: 0.316, 0.388; $P < 0.001$), while the association with tau burdens did not reach statistical significance ($n = 215$; beta 0.008/year; 95% CI: −0.017, 0.033; $P = 0.549$).

Discussion

Although MRI-based measures are widely viewed as candidate neurodegenerative disease biomarkers, little is known about the microscopic pathological signatures underlying changes in the MRI. Previous studies to address this issue have focused on structural MRI in Alzheimer's disease, and no information is available regarding imaging-to-pathology correlation in FTD or links between task-free functional MRI and neuropathological findings. Here, we capitalized on a large longitudinal series in which patients were followed from neuroimaging to death, allowing for a region-by-region comparison between magnetic resonance measures and neuropathology. The most important and novel finding of this study is the relationship between tau inclusion burden in PSP and CBD and the extent of antemortem brain atrophy, measured by brain MRI. This association proved independent of the local neurodegeneration severity. Our data suggest that the relationship between tau burden and magnetic resonance atrophy may be more driven by neuronal tau in PSP and by glial tau in CBD, but further study is needed to confirm these hypotheses. As expected, we also observed a significant association between the severity of neurodegeneration and MRI-based atrophy, independent of the tau inclusion burden in both our PSP and CBD cohorts. Taken together, these data suggest that *in vivo* structural imaging measures of regional brain atrophy may represent robust biomarkers of tau burden in PSP, CBD, and possibly other forms of neurodegeneration, even when imaging data are acquired years prior to death. These data may have important implication for ongoing and future clinical trials in which volumetric MRI parameters are used as secondary outcome measures (Boxer *et al.*, 2017).

Pathological tau protein deposition has been directly associated with neuronal loss (Gomez-Isla *et al.*, 1997; Giannakopoulos *et al.*, 2003) and grey matter atrophy (Jack *et al.*, 2002; Whitwell *et al.*, 2008) in Alzheimer's disease. Both regional tau deposition and grey matter atrophy are strong predictors of cognitive deficit in Alzheimer's disease (Arriagada *et al.*, 1992; Nelson *et al.*, 2012). Neuropathological studies have shown that the preferential involvement of selected anatomical areas by tau deposition is associated with the clinical and anatomical phenotypical expression of mild cognitive impairment and Alzheimer's disease (Hof *et al.*, 1989; Mitchell *et al.*, 2002; Guillozet *et al.*, 2003; Murray *et al.*, 2011; Gefen *et al.*, 2012), through mechanisms that may be in part independent from the severity of neuronal loss, gliosis and neuropil rarefaction (von Gunten *et al.*, 2006). A direct association between regional neuropathological tau burden and cognitive or structural changes has also been observed in primary age-related tauopathy (Josephs *et al.*, 2017). The recent availability of tau PET ligands allows the assessment of correlations between *in vivo* measures of tau deposition or regional extent with clinical findings. Tau deposition as assessed *in vivo* using ^{18}F-AV-1451 tau-PET predicts regional grey matter loss in Alzheimer's disease (Iaccarino *et al.*, 2018), the preferential involvement of distinct anatomical regions underlying the phenotypical variability of Alzheimer's disease (Ossenkoppele *et al.*, 2016), and the patterns of cortical volume loss in cognitively normal elder individuals (LaPoint *et al.*, 2017). More recently, a direct effect of regional ^{18}F-AV-1451 uptake on region-specific cognitive performance, in part independently from neurodegeneration, has been shown in a cohort of patients with Alzheimer's disease pathology (Bejanin *et al.*, 2017). Our data parallel the results of prior studies supporting the hypothesis of a direct effect of the regional tau severity in determining regional volume loss and related phenotypic disease manifestations in Alzheimer's disease, while providing unprecedented evidence of a similar association in non-Alzheimer primary tauopathies.

Tau aggregation in neurons has been associated with altered synaptic protein expression, and deficits in axonal transport that result in impaired trafficking of mitochondria and synaptic receptors to the synapses, and ultimately synaptic loss (Callahan *et al.*, 1999; Ginsberg *et al.*, 2000; Katsuse *et al.*, 2006; Spires-Jones and Hyman, 2014). We therefore predicted an association between regional tau inclusion burden and intrinsic connectivity dysfunction. Our data instead revealed only non-statistically significant relationships between neuropathologically assessed tauopathy and seed-based intrinsic connectivity dysfunction, when accounting for the extent of regional neurodegeneration and the interval time between imaging studies and death. Regional neurodegeneration predicted intrinsic connectivity dysfunction in the CBD group, while in PSP the association was in the expected direction, but did not reach statistical significance. Together our results suggest that single-subject, network-based intrinsic connectivity measures may face limitations in their use as biomarkers of post-mortem regional tau inclusion burden in PSP and CBD. Within-networks increased intrinsic connectivity has been reported in patients with a clinical diagnosis of PSP-RS or corticobasal syndrome, and postulated to represent increased baseline synchronization underlying within-network dysfunction (Bharti *et al.*, 2017). In addition, a positive correlation has been reported between average cortical connection strength and ^{18}F-AV-1451 uptake in patients with PSP-RS (Cope *et al.*, 2018). On the other hand, several seed-based intrinsic connectivity studies have shown within-network connectivity disruption in patients with PSP-RS or corticobasal syndrome (Whitwell *et al.*, 2011*a*; Gardner *et al.*, 2013; Piattella *et al.*, 2015; Upadhyay *et al.*, 2017). A recent longitudinal study of patients with PSP-RS showed that baseline intrinsic connectivity deficits are more evident

in regional hubs within the rostral midbrain tegmentum network but also that connectivity measures fail to predict or strongly correlate with longitudinal clinical decline (Brown *et al.*, 2017). In addition, the lack of association between pathological changes and measures of intrinsic connectivity in neurodegenerative diseases may depend on disease stages, with a possible direct association in the early disease stages, followed by a plateau phase once the severity of regional neurodegeneration reaches ceiling (Greicius *et al.*, 2004; Buckner *et al.*, 2005; Zhou *et al.*, 2008; Zhang *et al.*, 2010; Wang *et al.*, 2013). Taken together, these findings may explain why intrinsic connectivity measures may not correlate with post-mortem pathological measures. Alternatively, it is possible that both rostral midbrain tegmentum- and superior frontal sulcus-seeded regional connectivity networks maps are relatively variable in control individuals, a circumstance that would affect the sensitivity of the W-score approach. Further work may help clarify the optimal single-subject implementation of task-free functional MRI approaches.

Our study has several limitations including the relatively long interval between imaging and pathological assessment and the semi-quantitative nature of our neurodegeneration and tau inclusion burden measures, which are subject to ceiling effects in areas with severe pathological changes. In addition, the heterogeneous clinical presentations within the CBD cohort might have limited the strength of our seed-based connectivity analysis since the superior frontal sulcus may not have anchored the most relevant brain network in all of the patients with CBD.

Modelling imaging–pathology relationships using linear mixed effects presents specific challenges and required us to make several assumptions and simplifications (Baayen *et al.*, 2008). In that light, our findings, especially those of marginal statistical significance, should be interpreted with due caution. In our analysis, patients and region factors were both entered in the model as crossed random effects. This approach differs from that commonly used in brain imaging studies, where brain region is entered as a fixed effect. Unlike many brain imaging studies, however, our semi-quantitative neuropathological assessments were limited to a small set of regions, which are representative but not inclusive of the whole brain, and we have treated this set of regions as a random sample from the set of possible brain regions. This assumption creates a design with two random effects, which is not compatible with an ANOVA but instead calls for a linear mixed model. A linear mixed model further enables patient and region of interest effects to be crossed, rather than nested. This is an approximation since patient and region effects are unlikely to be completely independent. However, we favoured the crossed random-effect structure over a region-within-subject nested configuration, since the latter would not take into consideration the correlation that exists within a region across subjects. Considering region as a fixed effect would prevent incorporating the correlation between regions or the correlations between regions and subjects. The crossed random effects approach allows the mean of a response to depend on patient and region of interest random effects, as well as fixed effects. The risk of inflated type I error is modest (Barr *et al.*, 2013), and while noting the marginal significance of the confirmatory analysis regarding the link between tau inclusion burden and volume loss *in vivo*, it is unlikely to affect the principal inferences regarding the strong association between post mortem neurodegeneration and volume loss *in vivo*. Nevertheless, our study is the first to relate *in vivo* structural and functional imaging measures to pathological hallmarks in primary tauopathies.

In summary this study provides: (i) an unprecedented description of the association between non- Alzheimer neurodegenerative diseases and *in vivo* structural and functional connectivity imaging biomarkers; (ii) a replicable model for further assessment of the relationship between other proteinopathies and distinct imaging biomarkers; (iii) novel evidence of the value of structural brain MRI as a predictor of neurodegeneration and tau burden in primary tauopathies; and (iv) additional evidence for the complex relationship between proteinopathy burden and measures of intrinsic connectivity *in vivo*, which warrants caution when attempting to use this imaging methodology as a biomarker of microscopic pathology in clinical trials.

Acknowledgements

We are indebted to the research participants and their families for their generous contribution to science. We thank Norbert Lee, Caroline Prioleau, and Julian Ramirez for technical assistance.

Funding

This study was supported by grants P01AG019724 (B.L.M.), P50AG023501 (B.L.M.), K08AG052648 (S.S.), K01AG055698 (J.A.B.), K24AG053435 (L.T.G.), U54NS092089 (A.L.B.), R01AG022983 (J.H.K.), R01AG 032289 (J.H.K.), R01AG038791 (A.L.B.), R01EB022055 (J.K.) from the NIH National Institutes of Health, as well as the Tau Consortium (W.W.S.), Bluefield Project to Cure FTD (W.W.S), and Corticobasal Degeneration Solutions (A.L.B.).

Competing interests

The authors report no competing interests.

Supplementary material

Supplementary material is available at *Brain* online.

References

Armstrong MJ, Litvan I, Lang AE, Bak TH, Bhatia KP, Borroni B, et al. Criteria for the diagnosis of corticobasal degeneration. Neurology 2013; 80: 496–503.

Arriagada PV, Growdon JH, Hedley-Whyte ET, Hyman BT. Neurofibrillary tangles but not senile plaques parallel duration and severity of Alzheimer's disease. Neurology 1992; 42(Pt 1): 631–9.

Baayen RH, Davidson DJ, Bates DM. Mixed-effects modeling with crossed random effects for subjects and items. J Mem Lang 2008; 59: 390–412.

Bacchetti P. Peer review of statistics in medical research: the other problem. BMJ 2002; 324: 1271–3.

Barr DJ, Levy R, Scheepers C, Tily HJ. Random effects structure for confirmatory hypothesis testing: Keep it maximal. J Mem Lang 2013; 68: 255–78.

Bejanin A, Schonhaut DR, La Joie R, Kramer JH, Baker SL, Sosa N, et al. Tau pathology and neurodegeneration contribute to cognitive impairment in Alzheimer's disease. Brain 2017; 140: 3286–300.

Bharti K, Bologna M, Upadhyay N, Piattella MC, Suppa A, Petsas N, et al. Abnormal resting-state functional connectivity in progressive supranuclear palsy and corticobasal syndrome. Front Neurol 2017; 8: 248.

Borroni B, Alberici A, Cercignani M, Premi E, Serra L, Cerini C, et al. Granulin mutation drives brain damage and reorganization from preclinical to symptomatic FTLD. Neurobiology of aging 2012; 33: 2506–20.

Boxer AL, Geschwind MD, Belfor N, Gorno-Tempini ML, Schauer GF, Miller BL, et al. Patterns of brain atrophy that differentiate corticobasal degeneration syndrome from progressive supranuclear palsy. Archives of neurology 2006; 63: 81–6.

Boxer AL, Yu JT, Golbe LI, Litvan I, Lang AE, Hoglinger GU. Advances in progressive supranuclear palsy: new diagnostic criteria, biomarkers, and therapeutic approaches. Lancet Neurol 2017; 16: 552–63.

Braak H, Braak E. Neuropathological stageing of Alzheimer-related changes. Acta Neuropathol 1991; 82: 239–59.

Brown JA, Hua AY, Trujllo A, Attygalle S, Binney RJ, Spina S, et al. Advancing functional dysconnectivity and atrophy in progressive supranuclear palsy. NeuroImage Clin 2017; 16: 564–74.

Buckner RL, Snyder AZ, Shannon BJ, LaRossa G, Sachs R, Fotenos AF, et al. Molecular, structural, and functional characterization of Alzheimer's disease: evidence for a relationship between default activity, amyloid, and memory. J Neurosci 2005; 25: 7709–17.

Burton EJ, Barber R, Mukaetova-Ladinska EB, Robson J, Perry RH, Jaros E, et al. Medial temporal lobe atrophy on MRI differentiates Alzheimer's disease from dementia with Lewy bodies and vascular cognitive impairment: a prospective study with pathological verification of diagnosis. Brain 2009; 132 (Pt 1): 195–203.

Callahan LM, Vaules WA, Coleman PD. Quantitative decrease in synaptophysin message expression and increase in cathepsin D message expression in Alzheimer disease neurons containing neurofibrillary tangles. J Neuropathol Exp Neurol 1999; 58: 275–87.

Cash DM, Bocchetta M, Thomas DL, Dick KM, van Swieten JC, Borroni B, et al. Patterns of gray matter atrophy in genetic frontotemporal dementia: results from the GENFI study. Neurobiol Aging 2018; 62: 191–6.

Clavaguera F, Bolmont T, Crowther RA, Abramowski D, Frank S, Probst A, et al. Transmission and spreading of tauopathy in transgenic mouse brain. Nature Cell Biol 2009; 11: 909–13.

Collins JA, Montal V, Hochberg D, Quimby M, Mandelli ML, Makris N, et al. Focal temporal pole atrophy and network degeneration in semantic variant primary progressive aphasia. Brain 2017; 140: 457–71.

Cope TE, Rittman T, Borchert RJ, Jones PS, Vatansever D, Allinson K, et al. Tau burden and the functional connectome in Alzheimer's disease and progressive supranuclear palsy. Brain 2018; 141: 550–67.

de Calignon A, Polydoro M, Suarez-Calvet M, William C, Adamowicz DH, Kopeikina KJ, et al. Propagation of tau pathology in a model of early Alzheimer's disease. Neuron 2012; 73: 685–97.

de Silva R, Lashley T, Gibb G, Hanger D, Hope A, Reid A, et al. Pathological inclusion bodies in tauopathies contain distinct complements of tau with three or four microtubule-binding repeat domains as demonstrated by new specific monoclonal antibodies. Neuropathol Appl Neurobiol 2003; 29: 288–302.

Dickson DW, Bergeron C, Chin SS, Duyckaerts C, Horoupian D, Ikeda K, et al. Office of Rare Diseases neuropathologic criteria for corticobasal degeneration. J Neuropathol Exp Neurol 2002; 61: 935–46.

Fahn S, Elton RL, Development Committee U. The unified Parkinson's disease rating scale. In: Fahn S, Marsden CD, Calne DB, Goldstein M, editors. Recent developments in Parkinson's disease. Florham Park, NJ: Macmillan Healthcare Information; 1987. p. 153–63, 293–304.

Fan L, Li H, Zhuo J, Zhang Y, Wang J, Chen L, et al. The human brainnetome atlas: a new brain atlas based on connectional architecture. Cerebral Cortex 2016; 26: 3508–26.

Farb NA, Grady CL, Strother S, Tang-Wai DF, Masellis M, Black S, et al. Abnormal network connectivity in frontotemporal dementia: evidence for prefrontal isolation. Cortex 2013; 49: 1856–73.

Ferrer I, Santpere G, van Leeuwen FW. Argyrophilic grain disease. Brain 2008; 131(Pt 6): 1416–32.

Filippi M, Agosta F, Scola E, Canu E, Magnani G, Marcone A, et al. Functional network connectivity in the behavioral variant of frontotemporal dementia. Cortex 2013; 49: 2389–401.

Gardner RC, Boxer AL, Trujillo A, Mirsky JB, Guo CC, Gennatas ED, et al. Intrinsic connectivity network disruption in progressive supranuclear palsy. Ann Neurol 2013; 73: 603–16.

Gefen T, Gasho K, Rademaker A, Lalehzari M, Weintraub S, Rogalski E, et al. Clinically concordant variations of Alzheimer pathology in aphasic versus amnestic dementia. Brain 2012; 135(Pt 5): 1554–65.

Giannakopoulos P, Herrmann FR, Bussiere T, Bouras C, Kovari E, Perl DP, et al. Tangle and neuron numbers, but not amyloid load, predict cognitive status in Alzheimer's disease. Neurology 2003; 60: 1495–500.

Gil MJ, Manzano MS, Cuadrado ML, Fernandez C, Gomez E, Matesanz C, et al. Argyrophilic grain pathology in frontotemporal lobar degeneration: demographic, clinical, neuropathological, and genetic features. J Alzheimer's Dis 2018; 63: 1109–17.

Ginsberg SD, Hemby SE, Lee VM, Eberwine JH, Trojanowski JQ. Expression profile of transcripts in Alzheimer's disease tangle-bearing CA1 neurons. Ann Neurol 2000; 48(1): 77–87.

Gomez-Isla T, Hollister R, West H, Mui S, Growdon JH, Petersen RC, et al. Neuronal loss correlates with but exceeds neurofibrillary tangles in Alzheimer's disease. Ann Neurol 1997; 41: 17–24.

Goveas JS, Xie C, Ward BD, Wu Z, Li W, Franczak M, et al. Recovery of hippocampal network connectivity correlates with cognitive improvement in mild Alzheimer's disease patients treated with donepezil assessed by resting-state fMRI. J Magn Reson Imaging 2011; 34: 764–73.

Greicius MD, Srivastava G, Reiss AL, Menon V. Default-mode network activity distinguishes Alzheimer's disease from healthy aging: evidence from functional MRI. Proc Natl Acad Sci USA 2004; 101: 4637–42.

Guillozet AL, Weintraub S, Mash DC, Mesulam MM. Neurofibrillary tangles, amyloid, and memory in aging and mild cognitive impairment. Arch Neurol 2003; 60: 729–36.

Guo CC, Gorno-Tempini ML, Gesierich B, Henry M, Trujillo A, Shany-Ur T, et al. Anterior temporal lobe degeneration produces widespread network-driven dysfunction. Brain 2013; 136(Pt 10): 2979–91.

Hoenig MC, Bischof GN, Seemiller J, Hammes J, Kukolja J, Onur OA, et al. Networks of tau distribution in Alzheimer's disease. Brain 2018; 141: 568–81.

Höglinger GU, Respondek G, Stamelou M, et al. Clinical diagnosis of progressive supranuclear palsy: the movement disorder society criteria. Mov Disord 2017; 32: 853–64.

Hof PR, Bouras C, Constantinidis J, Morrison JH. Balint's syndrome in Alzheimer's disease: specific disruption of the occipito-parietal visual pathway. Brain Res 1989; 493: 368–75.

Hyman BT, Van Hoesen GW, Damasio AR, Barnes CL. Alzheimer's disease: cell-specific pathology isolates the hippocampal formation. Science 1984; 225: 1168–70.

Iaccarino L, Tammewar G, Ayakta N, Baker SL, Bejanin A, Boxer AL, et al. Local and distant relationships between amyloid, tau and neurodegeneration in Alzheimer's Disease. NeuroImage Clinical 2018; 17: 452–64.

Jack CR Jr, Dickson DW, Parisi JE, Xu YC, Cha RH, O'Brien PC, et al. Antemortem MRI findings correlate with hippocampal neuropathology in typical aging and dementia. Neurology 2002; 58: 750–7.

Jack CR Jr, Knopman DS, Jagust WJ, Petersen RC, Weiner MW, Aisen PS, et al. Tracking pathophysiological processes in Alzheimer's disease: an updated hypothetical model of dynamic biomarkers. Lancet Neurol 2013; 12: 207–16.

Josephs KA, Murray ME, Tosakulwong N, Whitwell JL, Knopman DS, Machulda MM, et al. Tau aggregation influences cognition and hippocampal atrophy in the absence of beta-amyloid: a clinico-imaging-pathological study of primary age-related tauopathy (PART). Acta neuropathologica 2017; 133: 705–15.

Katsuse O, Lin WL, Lewis J, Hutton ML, Dickson DW. Neurofibrillary tangle-related synaptic alterations of spinal motor neurons of P301L tau transgenic mice. Neuroscience letters 2006; 409: 95–9.

La Joie R, Perrotin A, Barre L, Hommet C, Mezenge F, Ibazizene M, et al. Region-specific hierarchy between atrophy, hypometabolism, and beta-amyloid (Abeta) load in Alzheimer's disease dementia. J Neurosci 2012; 32: 16265–73.

LaPoint MR, Chhatwal JP, Sepulcre J, Johnson KA, Sperling RA, Schultz AP. The association between tau PET and retrospective cortical thinning in clinically normal elderly. NeuroImage 2017; 157: 612–22.

Litvan I, Agid Y, Calne D, Campbell G, Dubois B, Duvoisin RC, et al. Clinical research criteria for the diagnosis of progressive supranuclear palsy (Steele-Richardson-Olszewski syndrome): report of the NINDS-SPSP international workshop. Neurology 1996a; 47: 1–9.

Litvan I, Hauw JJ, Bartko JJ, Lantos PL, Daniel SE, Horoupian DS, et al. Validity and reliability of the preliminary NINDS neuropathologic criteria for progressive supranuclear palsy and related disorders. J Neuropathol Exp Neurol 1996b; 55: 97–105.

Liu L, Drouet V, Wu JW, Witter MP, Small SA, Clelland C, et al. Trans-synaptic spread of tau pathology in vivo. PLoS One 2012; 7: e31302.

Mackenzie IR, Neumann M, Bigio EH, Cairns NJ, Alafuzoff I, Kril J, et al. Nomenclature and nosology for neuropathologic subtypes of frontotemporal lobar degeneration: an update. Acta neuropathologica 2010a; 119: 1–4.

Mackenzie IR, Rademakers R, Neumann M. TDP-43 and FUS in amyotrophic lateral sclerosis and frontotemporal dementia. Lancet neurology 2010b; 9: 995–1007.

Mandelli ML, Vilaplana E, Brown JA, Hubbard HI, Binney RJ, Attygalle S, et al. Healthy brain connectivity predicts atrophy progression in non-fluent variant of primary progressive aphasia. Brain 2016; 139(Pt 10): 2778–91.

McKeith IG, Galasko D, Kosaka K, Perry EK, Dickson DW, Hansen LA, et al. Consensus guidelines for the clinical and pathologic diagnosis of dementia with Lewy bodies (DLB): report of the consortium on DLB international workshop. Neurology 1996; 47: 1113–24.

Mitchell TW, Mufson EJ, Schneider JA, Cochran EJ, Nissanov J, Han LY, et al. Parahippocampal tau pathology in healthy aging, mild cognitive impairment, and early Alzheimer's disease. Ann Neurol 2002; 51: 182–9.

Montine TJ, Phelps CH, Beach TG, Bigio EH, Cairns NJ, Dickson DW, et al. National Institute on Aging-Alzheimer's Association guidelines for the neuropathologic assessment of Alzheimer's disease: a practical approach. Acta Neuropathol 2012; 123: 1–11.

Murray ME, Graff-Radford NR, Ross OA, Petersen RC, Duara R, Dickson DW. Neuropathologically defined subtypes of Alzheimer's disease with distinct clinical characteristics: a retrospective study. The Lancet Neurology 2011; 10: 785–96.

Nelson PT, Alafuzoff I, Bigio EH, Bouras C, Braak H, Cairns NJ, et al. Correlation of Alzheimer disease neuropathologic changes with cognitive status: a review of the literature. J Neuropathol Exp Neurol 2012; 71: 362–81.

Ossenkoppele R, Schonhaut DR, Scholl M, Lockhart SN, Ayakta N, Baker SL, et al. Tau PET patterns mirror clinical and neuroanatomical variability in Alzheimer's disease. Brain 2016; 139(Pt 5): 1551–67.

Perneger TV. What's wrong with Bonferroni adjustments. BMJ 1998; 316: 1236–8.

Perry DC, Brown JA, Possin KL, Datta S, Trujillo A, Radke A, et al. Clinicopathological correlations in behavioural variant frontotemporal dementia. Brain 2017; 140: 3329–45.

Pfeffer RI, Kurosaki TT, Harrah CH, Jr., Chance JM, Filos S. Measurement of functional activities in older adults in the community. J Gerontol 1982; 37: 323–9.

Piattella MC, Tona F, Bologna M, Sbardella E, Formica A, Petsas N, et al. Disrupted resting-state functional connectivity in progressive supranuclear palsy. Am J Neuroradiol 2015; 36: 915–21.

Pievani M, Paternico D, Benussi L, Binetti G, Orlandini A, Cobelli M, et al. Pattern of structural and functional brain abnormalities in asymptomatic granulin mutation carriers. Alzheimer's Dement 2014; 10(Suppl 5): S354–63.e1

Raj A, Kuceyeski A, Weiner M. A network diffusion model of disease progression in dementia. Neuron 2012; 73: 1204–15.

Raman MR, Schwarz CG, Murray ME, Lowe VJ, Dickson DW, Jack CR Jr., et al. An MRI-based atlas for correlation of imaging and pathologic findings in Alzheimer's disease. J Neuroimaging 2016; 26: 264–8.

Rascovsky K, Hodges JR, Knopman D, Mendez MF, Kramer JH, Neuhaus J, et al. Sensitivity of revised diagnostic criteria for the behavioural variant of frontotemporal dementia. Brain 2011; 134(Pt 9): 2456–77.

Rodriguez RD, Suemoto CK, Molina M, Nascimento CF, Leite RE, de Lucena Ferretti-Rebustini RE, et al. Argyrophilic grain disease: demographics, clinical, and neuropathological features from a large autopsy study. J Neuropathol Exp Neurol 2016; 75: 628–35.

Rohrer JD, Nicholas JM, Cash DM, van Swieten J, Dopper E, Jiskoot L, et al. Presymptomatic cognitive and neuroanatomical changes in genetic frontotemporal dementia in the Genetic Frontotemporal dementia Initiative (GENFI) study: a cross-sectional analysis. Lancet Neurol 2015; 14: 253–62.

Rorden C, Brett M. Stereotaxic display of brain lesions. Behav Neurol 2000; 12: 191–200.

Rothman KJ. No adjustments are needed for multiple comparisons. Epidemiology 1990; 1: 43–6.

Savitz DA, Olshan AF. Multiple comparisons and related issues in the interpretation of epidemiologic data. Am J Epidemiol 1995; 142: 904–8.

Seeley WW, Crawford RK, Zhou J, Miller BL, Greicius MD. Neurodegenerative diseases target large-scale human brain networks. Neuron 2009; 62: 42–52.

Seeley WW, Menon V, Schatzberg AF, Keller J, Glover GH, Kenna H, et al. Dissociable intrinsic connectivity networks for salience processing and executive control. J Neurosci 2007; 27: 2349–56.

Serra L, Cercignani M, Mastropasqua C, Torso M, Spano B, Makovac E, et al. Longitudinal changes in functional brain connectivity predicts conversion to Alzheimer's disease. J Alzheimer's Dis 2016; 51: 377–89.

Sperling R, Mormino E, Johnson K. The evolution of preclinical Alzheimer's disease: implications for prevention trials. Neuron 2014; 84: 608–22.

Spires-Jones TL, Hyman BT. The intersection of amyloid beta and tau at synapses in Alzheimer's disease. Neuron 2014; 82: 756–71.

Tartaglia MC, Sidhu M, Laluz V, Racine C, Rabinovici GD, Creighton K, et al. Sporadic corticobasal syndrome due to FTLD-TDP. Acta Neuropathol 2010; 119: 365–74.

Upadhyay N, Suppa A, Piattella MC, Gianni C, Bologna M, Di Stasio F, et al. Functional disconnection of thalamic and cerebellar dentate nucleus networks in progressive supranuclear palsy and corticobasal syndrome. Parkinson Relat Disord 2017; 39: 52–7.

von Gunten A, Kovari E, Bussiere T, Rivara CB, Gold G, Bouras C, et al. Cognitive impact of neuronal pathology in the entorhinal cortex and CA1 field in Alzheimer's disease. Neurobiol Aging 2006; 27: 270–7.

Wang Y, Risacher SL, West JD, McDonald BC, Magee TR, Farlow MR, et al. Altered default mode network connectivity in older adults with cognitive complaints and amnestic mild cognitive impairment. J Alzheimer's Disord 2013; 35: 751–60.

Whitwell JL, Avula R, Master A, Vemuri P, Senjem ML, Jones DT, et al. Disrupted thalamocortical connectivity in PSP: a resting-state fMRI, DTI, and VBM study. Parkinson Relat Disord 2011a; 17: 599–605.

Whitwell JL, Hoglinger GU, Antonini A, Bordelon Y, Boxer AL, Colosimo C, et al. Radiological biomarkers for diagnosis in PSP: Where are we and where do we need to be? Mov Disord 2017; 32: 955–71.

Whitwell JL, Josephs KA, Avula R, Tosakulwong N, Weigand SD, Senjem ML, et al. Altered functional connectivity in asymptomatic MAPT subjects: a comparison to bvFTD. Neurology 2011b; 77: 866–74.

Whitwell JL, Josephs KA, Murray ME, Kantarci K, Przybelski SA, Weigand SD, et al. MRI correlates of neurofibrillary tangle pathology at autopsy: a voxel-based morphometry study. Neurology 2008; 71: 743–9.

Zhang HY, Wang SJ, Liu B, Ma ZL, Yang M, Zhang ZJ, et al. Resting brain connectivity: changes during the progress of Alzheimer disease. Radiology 2010; 256: 598–606.

Zhou J, Gennatas ED, Kramer JH, Miller BL, Seeley WW. Predicting regional neurodegeneration from the healthy brain functional connectome. Neuron 2012; 73: 1216–27.

Zhou J, Greicius MD, Gennatas ED, Growdon ME, Jang JY, Rabinovici GD, et al. Divergent network connectivity changes in behavioural variant frontotemporal dementia and Alzheimer's disease. Brain 2010; 133(Pt 5): 1352–67.

Zhou J, Liu S, Ng KK, Wang J. Applications of resting-state functional connectivity to neurodegenerative disease. Neuroimaging Clin North Am 2017; 27: 663–83.

Zhou Y, Dougherty JH, Jr., Hubner KF, Bai B, Cannon RL, Hutson RK. Abnormal connectivity in the posterior cingulate and hippocampus in early Alzheimer's disease and mild cognitive impairment. Alzheimer's Dement 2008; 4: 265–70.